Journal of Zhejiang University-SCIENCE A (Applied Physics & Engineering) in press
www.jzus.zju.edu.cn; www.springer.com/journal/11582
E-mail: jzus_a@zju.edu.cn

Research Article

https://doi.org/10.1631/jzus.A2400407

A grid-growth method for the reconstruction of 3D rock joints with arbitrary joint roughness and persistence

Hanyu CHEN, Peng GUO, Guangyao LI, Lifen FAN✉

Architecture and Civil Engineering, Beijing University of Technology, Beijing 100124, China

Abstract: We present a grid-growth method to reconstruct 3D rock joints with arbitrary joint roughness and persistence. In the first step of this workflow, the joint model is divided into uniform grids. Then by adjusting the positions of the grids, the joint morphology can be modified to construct models with desired joint roughness and persistence. Accordingly, numerous joint models with different joint roughness and persistence were built. The effects of relevant parameters (such as the number, height, and slope of asperities, and the number and area of rock bridges) on the joint roughness coefficient (JRC) and joint persistence were investigated. Finally, an artificially split joint was reconstructed using the method, and the method's accuracy was evaluated by comparing the JRC of the models with that of the artificially split joint. The results showed that the proposed method can effectively control the JRC of joint models by adjusting the number, height, and slope of asperities. The method can also modify the persistence of joint models by adjusting the number and area of rock bridges. Additionally, the JRC of models obtained by our method agree with that of the artificially split surface. Overall, the method demonstrated high accuracy for 3D rock joint reconstruction.

Key words: 3D rock joint reconstruction; Joint roughness; Joint persistence; Asperity; Rock bridge

1 Introduction

Rock joints exist in a variety of natural rock masses. The mechanical properties of rock joints are closely related to the stability of the rock mass. Furthermore, studies have revealed that the mechanical properties of rock joints are strongly influenced by the joint surface morphology (Barton and Choubey, 1977; Tse and Cruden, 1979; Gentier et al., 2000; Huang et al., 2014; Le et al., 2018; Thomas et al., 2021). Therefore, the reconstruction of joint surface morphology is of great significance to rock mass stability analysis (Marache et al., 2002; Liu et al., 2017; Zhao et al., 2020; Song et al., 2022).

In general, rock joints can be classified into two categories: persistent and non-persistent joints. A large number of studies have focused on the reconstruction of these two types of rock joints. For persistent joints, the joint roughness is of primary concern. Two methods are commonly used for rough rock joint reconstruction in 2D and 3D. The first method involves scanning the natural rock joints to obtain the surface morphology and generate a corresponding digital model. For example, using 3D scanning, computer-aided design (CAD), and digital image processing, virtual rock joint models with realistic morphological characteristics have been successfully reconstructed (Jiang et al., 2016; Zhang et al., 2016; Xue et al., 2020; Liu et al., 2024). To sidestep the high cost of 3D scanning, this method was improved to reconstruct 3D rock joints based on 2D profiles (Liu et al., 2022a). However, the usable size of the rock samples is limited by the resolution and scanning range of the instruments (Lang et al., 2024). For large-scale rock joints, which are difficult to scan, another type of reconstruction method is required.

The second type of rock joint reconstruction method involves the use of algorithms. This approach first requires a quantitative description of the rough rock joints. Scholars have established ten typical joint profiles with different joint roughness coefficients (Barton and Choubey, 1977). The joint roughness coefficient can be determined by visual comparison with typical joint profiles. However due to the high subjectivity of this method, several parameters have

✉ Lifeng FAN, fanlifeng@bjut.edu.cn

Received Aug. 19, 2024; Revision accepted Sept. 23, 2024;
Crosschecked

been proposed to quantify the joint roughness coefficient, such as the root mean square Z_2, the structure function *SF* (Tse and Cruden, 1979; Gao and Wong, 2015), the roughness profile index R_P (Maerz et al., 1990), the roughness metric $\theta^*_{max}/(C+1)$ (Tatone and Grasselli, 2010), and the fractal dimension (Askari and Ahmadi, 2007; Bae et al., 2011). Using the above parameters, various rough rock joint reconstruction studies were performed. For the reconstruction of 2D rock joint profiles, a method based on Fourier series was proposed (Yong et al., 2018; Nie et al., 2019). This method successfully controlled the joint roughness by adjusting the Fourier amplitudes. For the reconstruction of 3D rock joint surfaces, a bubbling method was developed (Liu et al., 2022b). In this way, 3D rock joint surfaces with different roughness values in two orthogonal directions were successfully reconstructed. In addition, an alternative method using fractal theory was also effective for rock joint reconstruction in 2D and 3D (Zhou and Xie, 2003; Cattania and Segall, 2020). This method requires fewer iterations and thus improved the efficiency.

Non-persistent joints have also received significant research attention (Einstein et al., 1983; Shang et al., 2018). A series of geophysical measurements (Olsson et al., 1992; Tronicke and Knoll, 2005; Heike et al., 2008) and surface terrestrial laser scans (Sturzenegger and Stead, 2009) were performed to explore non-persistent rock joints. Based on this exploration, quantifiable parameters for joint persistence in 2D and 3D were defined (Kin et al., 2007; Prudencio and Van Sint Jan, 2007; Wasantha et al., 2014). Subsequently, numerous studies on non-persistent rock joint reconstruction were conducted. For example, 2D non-persistent rock joint models were successfully constructed via the discrete element method (Ghazvinian et al., 2012). To further consider the inhomogeneity and randomness of the rock bridge distribution, statistical analysis was performed on the geometric parameters of these joints (Song, 2006; Jimenez-Rodriguez and Sitar, 2006; Wu et al., 2011). Non-persistent rock joint reconstruction methods based on random distribution techniques were developed, such as the Monte Carlo (Wang et al., 2016) and discrete fracture network (Liu et al., 2015; Lei et al., 2017; Huang et al., 2023) methods. The effects of different geometric parameters on the mechanical properties of non-persistent joints were thus investigated. Then, study of non-persistent rock joints was extended to three dimensions. For example, 3D non-persistent rock joint models with randomly shaped rock bridges were built via the 3D particle flow modelling approach (Bahaaddini et al., 2016; Cao et al., 2022). At present, the majority of research on non-persistent joints concentrates on joint persistence, and assumes that the surfaces of non-persistent joints are smooth. However, there is still a lack of 3D rock joint reconstruction methods that consider both joint roughness and persistence.

Accordingly, in this study we propose a grid-growth method to reconstruct 3D rock joints with arbitrary joint roughness and persistence. A series of joint models with different joint roughness and persistence is reconstructed using the novel grid-growth method. The effects of the modelling parameters on the joint roughness coefficient (JRC) and joint persistence are subsequently investigated. Additionally, an artificially-split joint is reconstructed. Finally, by comparing the JRC of the models with that of the artificially-split joint, the accuracy of the proposed method is evaluated.

2 Method for 3D rock joint reconstruction

2.1 The grid-growth method

Generally, joint roughness and persistence are the most significant quantitative indicators of joint surface morphology. We present a reconstruction method for 3D rock joints with arbitrary roughness and persistence. The method is divided into three parts: orientation control, asperity generation, and rock bridge generation, as shown in Fig. 1. In the process of orientation control, a smooth and flat joint surface is constructed, which can be rotated in any direction. Thus, the size and the inclination of the rock joint model can both be controlled. In the process of asperity generation, the rough joint surface will be constructed by the algorithm to replace the original flat joint surface. The roughness of the rock joint model can also be controlled. In the process of rock bridge generation, randomly shaped and distributed areas on the rough joint surface are removed to simulate rock bridges. Moreover, the persistence of the rock joint model can be adjusted.

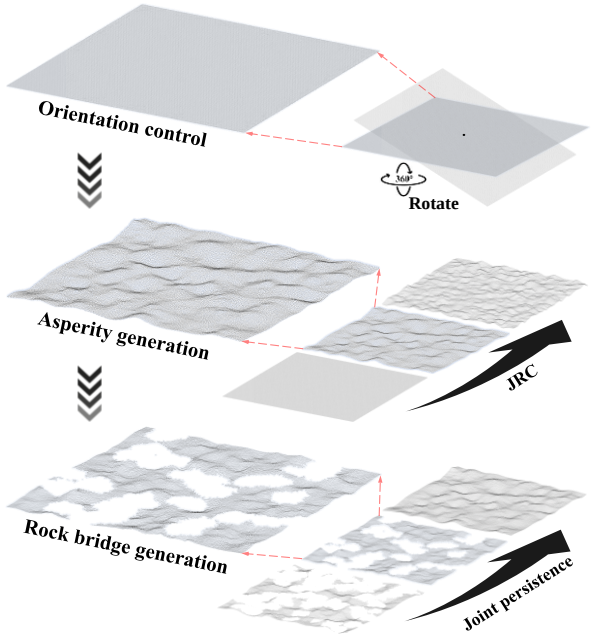

Fig. 1 Grid-growth method for the 3D rock joint reconstruction

The first part of the method (orientation control) is easily achieved by creating and rotating a flat joint surface. The second and third parts of the method (asperity generation and rock bridge generation) require more attention, as the randomness of the joint surface morphology must be accounted for. The traditional Quartet Structure Generation Set method provides a potential solution to the problem of the randomness of the joint surface morphology. According to previous studies, the Quartet Structure Generation Set method is a random internal morphology and structure generation-growth method, which is used to generate microstructures of porous media (Wang et al., 2007; Guan et al., 2015; Wang et al., 2019). Specifically, a grid system is set up to divide the model space into numerous grids. Then, some of the grids are selected as growing phases, and the growing phases grow randomly to generate the internal morphology. In this study, a similar idea of random growth is introduced to consider the randomness of the joint surface morphology. Thus, the model of the 3D rock joint will be divided into uniform grids. The final morphology of the rock joint model is then determined by the growth of the grids. Intuitively, this reconstruction method is called the grid-growth method.

2.2 The asperity generation method

Here, an algorithm for asperity generation is developed to transform a smooth and flat joint surface into a rough joint surface, as shown in Fig. 2. The algorithm consists of several steps as follows.

First, we uniformly divide the flat joint surface into grids, as shown in Figs. 2a and 2b. Note that the size of the grids should be small enough to ensure the accuracy of the final model. The size of the grids used in this study is 1/400 of the minimum side length of the plane.

Second, we randomly select two types of grids (convex and concave) from all the grids, as shown in Fig. 2c. For selection, a random number in the range from 0 to 1 is assigned to each grid in the region. Meanwhile, a parameter called the distribution probability of asperities (P_{Da}) is set. The grids with a random number less than $P_{Da}/2$ are defined as convex grids, and those with a number in the range from $P_{Da}/2$ to P_{Da} are defined as concave grids.

Third, we set an initial height for each convex grid or concave grid to form a 3D rectangular element; this is called the growth element. The growth elements will grow around its five surrounding directions, as shown in Fig. 2d. The growth elements of convex grids can grow vertically upwards and horizontally in the frontward, backward, leftward, and rightward directions. The growth elements of concave grids can grow vertically downwards and horizontally in the same four directions. To avoid overlapping of the growth elements, downward growth is not allowed for the growth elements of convex grids, and upward growth is not allowed for the growth elements of concave grids.

Fourth, we allow the growth elements to grow in the prescribed growth direction. For each growth element, the growth directions are randomly selected from its five surrounding directions. To determine the growth directions, a random number in the range from 0 to 1 is assigned to each direction. Meanwhile, a parameter called the growth probability of asperities (P_{Ga}) is set. The directions with a random number less than P_{Ga} are selected as the growth direction. New growth elements with the same size as the original growth element will accordingly be generated in the selected directions. The distance of each lateral growth extent is equal to the lateral side length of the growth element, and the distance of each vertical growth extent is equal to the height of the

growth element. If a growth element already exists in the selected direction, the growth fails. Additionally, this process follows two more rules. One is that the vertical growth only occurs in the vertical direction of the convex grids or the concave grids. The other is that a growth element must already exist at the bottom or top of each new growth element, otherwise the growth will fail.

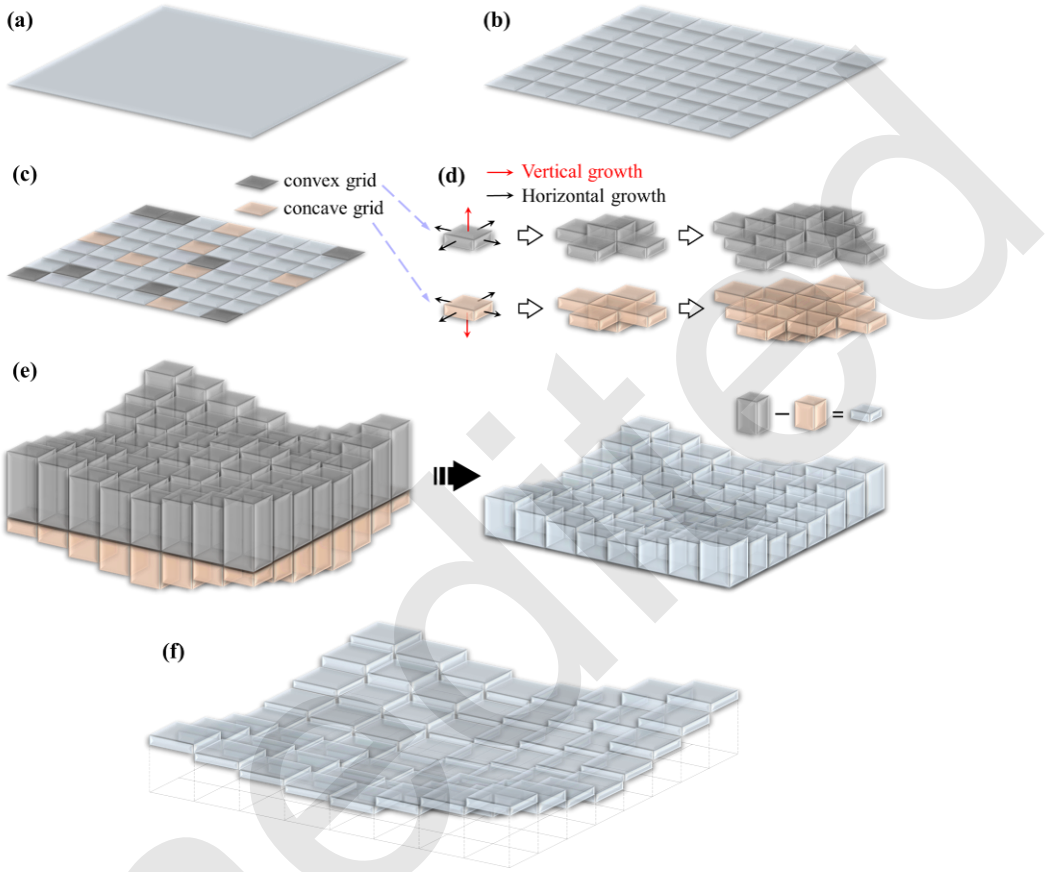

Fig. 2 Detailed explanation of the asperity generation. (a) The smooth and flat joint surface; (b) The uniform grids of the joint surface; (c) The convex grids and the concave grids; (d) The growth elements and the growth directions; (e) The model after the grid growth; (f) The rough rock joint model.

Next, we calculate the cumulative height in the vertical direction of each grid. The cumulative height is equal to the difference between the height above the original plane and the height below the original plane, as shown in Fig. 2e.

Finally, the fourth and fifth steps are repeated until the maximum of the cumulative height reaches the set maximum elevation difference (Δz_{Max}). Next, a plane is created at the cumulative height of the vertical direction of each grid. All the planes at different heights together form the rough joint surface, as shown in Fig. 2f.

In this algorithm, the slope of asperities is determined by the ratio of the height to the lateral side length of the growth element. Since the lateral side length of a growth element is constant, the slope of asperities can be controlled by adjusting the height of the growth element. Considering the randomness of the slope of the asperities in realistic conditions, the height of the growth element belonging to different grids is set to vary in this algorithm. In general, the slope angle of asperities on the joint surface along a certain direction (called the climbing angle) tends to follow a normal distribution (Liu et al., 2022b). Therefore, we set up a normal distribution function to determine the climbing angle and the slope of each asperity, where μ is the mean of the climbing angles, and σ is their standard deviation.

In summary, the asperity generation algorithm involves five parameters (P_{Da}, P_{Ga}, Δz_{Max}, μ, and σ). P_{Da} is used to select the convex grids and the concave grids. The value of P_{Da} determines the number of the

convex grids and the concave grids. P_{Ga} is used to select the growth directions of the growth elements, which ensure the randomness of the growth. It should be noted that the P_{Ga} of each growth direction is equal. When the value of P_{Ga} is close to 1, the shape of the asperities is regular. Conversely, the shape of the asperities is highly random when the value of P_{Ga} is close to 0. Δz_{Max} is a threshold for determining the end of the cycle in the algorithm, which controls the maximum elevation difference of the rock joint model. μ and σ are the mean and the standard deviation of the normal distribution, respectively, which are used to control the slope of asperities. To ensure the convergence of the algorithm, the product of P_{Da} and the number of grids should be greater than 1. In addition, a scaling coefficient can be set to cause a difference between the growth probability of upward and downward growth. This can also ensure the convergence of the algorithm.

2.3 The rock bridge generation method

In general, the joint persistence is defined as the ratio of the area of the discontinuous region to the total area of the rock joint surface (Cao et al., 2022). Due to the difficulty of measuring the area of the irregular rock joint surface, the projected plane is used to calculate joint persistence in this study. The relevant equation is:

$$K = \sum \left[\frac{S_J - S_{RBi}}{S_J} \right], \tag{1}$$

where K is the joint persistence, S_{RBi} is the projected area of the rock bridge, and S_J is the total area of the projection plane.

Also, an algorithm for the rock bridge generation is developed to control the joint persistence of the rock joint surface, as shown in Fig. 3. The algorithm consists of several steps as follows.

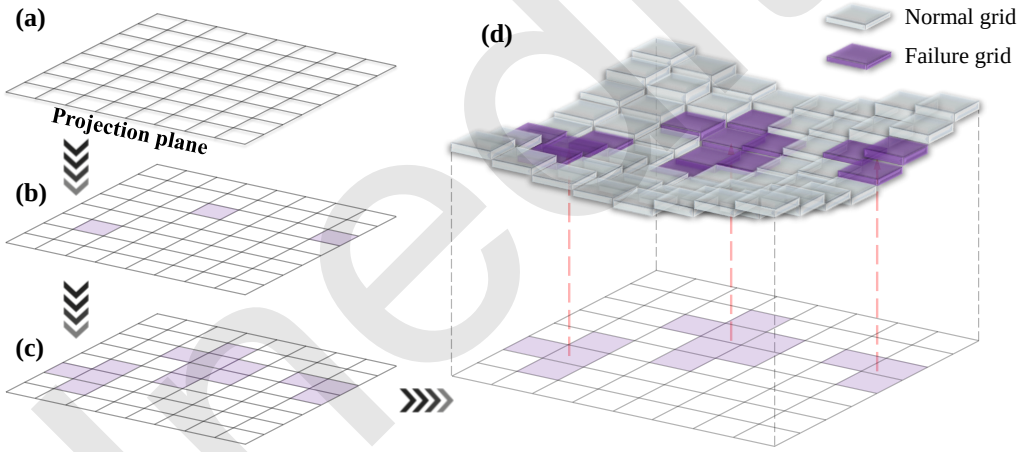

Fig. 3 Rock bridge generation. (a) The projection plane of the rock joint model; (b) The special grids on the projection plane; (c) The special grids after the grid growth; (d) The final 3D rock joint model.

First, a number of special grids are randomly selected from the rock joint projection plane, as shown in Figs. 3a and 3b. To select the grids, a random number in the range from 0 to 1 is assigned to each grid on the projection plane. Meanwhile, a parameter called the distribution probability of rock bridges (P_{Drb}) is set. The grids with a random number less than P_{Drb} are defined as the special grids.

Second, we allow the special grids to grow around their four surrounding directions within the projection plane, as shown in Fig. 3c. To select the growth directions, a random number in the range from 0 to 1 is assigned to each direction around the special grids. Meanwhile, a parameter called the growth probability of rock bridges (P_{Grb}) is set. The directions with a random number less than P_{Grb} are selected as the growth directions.

Third, the joint persistence is calculated using Eq. 1. The projected area of the rock bridges is equal to the area of the special grids. The total area of the projection plane is equal to the area of all grids within the projection plane.

Next, we repeat the second and third steps until the persistence of the rock joint reaches the set value of K_0.

Finally, we define the grids on the rough rock joint surfaces that correspond to the special grids as the failure grids, as shown in Fig. 3d. The failure

grids represent the region of rock bridges on the rough rock joint surfaces.

In summary, the rock bridge generation algorithm involves three parameters (P_{Drb}, P_{Grb}, and K_0). The P_{Drb} value is used to select the special grids and determine the number of special grids. The P_{Grb} value is used to select the growth directions of the special grids, which ensure the randomness of the growth. It should be noted that the P_{Grb} of each growth direction is the same. When the value of P_{Grb} is close to 1, the shape of the rock bridges is regular. Conversely, the shape of the rock bridges is highly random when the value of P_{Grb} is close to 0. The K_0 value is a threshold for determining the end of the cycle in the algorithm, which controls the joint persistence of the final model.

3 Results

Using the proposed grid-growth method, a 3D rock joint modelling software was established, as shown in Fig. 4a. The software enables parametric modelling of 3D rock joints and can output two types of models (solid models and point clouds) as illustrated in Fig. 4b. The point cloud is adopted in this study to demonstrate the 3D rock joint models, due to the shorter generation time and the convenience of the data statistics. In this section, the software is used to construct a series of 3D rock joint models with different joint roughness and persistence. The effects of the relevant modelling parameters on the joint roughness coefficient (JRC) and joint persistence are also investigated.

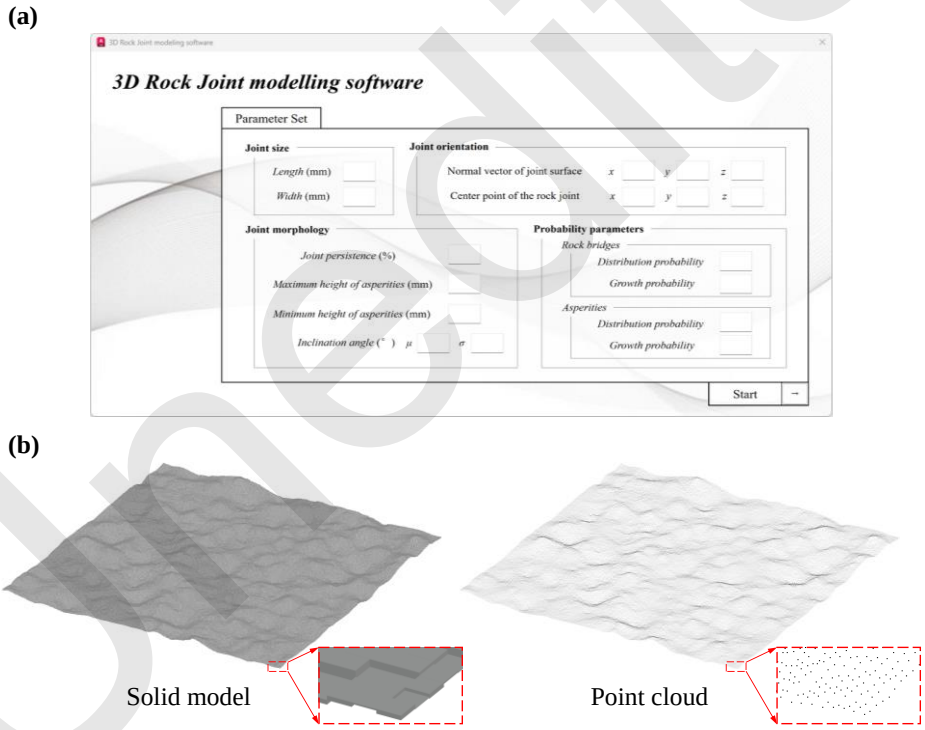

Fig. 4 3D rock joint modelling software and resulting models. (a) 3D rock joint modelling software; (b) Solid model and point cloud of the 3D rock joint.

In order to quantitatively characterize the roughness of 3D rock joints, the traditional quantification method (Tse and Cruden, 1979) is used to calculate the JRC of each 3D rock joint. A total of 201 profiles are selected at 0.5 mm intervals from the 3D rock joint surface for this method (Tatone and Grasselli, 2010; Liu et al., 2022b). The roughness of each profile is calculated by the empirical relationship between JRC and the root mean square Z_2 as follows:

$$\mathrm{JRC}^{2\mathrm{D}} = a + b\log Z_2, \tag{2}$$

The root mean square Z_2 is given as:

$$Z_2 = \left[\frac{1}{L}\int_{x=0}^{x=L}\left(\frac{dz}{dx}\right)^2 dx\right]^{1/2} = \left[\frac{1}{L}\sum_{i=1}^{N-1}\frac{(\Delta z)^2}{\Delta x}\right]^{1/2}, \quad (3)$$

where JRC^{2D} is the roughness of a single profile line, a and b are empirical coefficients (a = 32.2 and b = 32.47), Δx is the interval of sampling points along the profile line (0.5 mm in this study), Δz is the vertical difference between two adjacent points along the profile, L is the length of the contour projection, and N is the number of sampled points.

The overall roughness of the 3D rock joint surface is reflected by the average value of JRC^{2D} across all profile lines. The corresponding formula is:

$$\mathrm{JRC} = \frac{1}{201}\sum_{i=1}^{201}\left(\mathrm{JRC}^{2D}\right)_i, \quad (4)$$

where JRC is the joint roughness coefficient of the 3D rock joint.

Figs. 5–7 show the effects of three key modelling parameters (P_{Da}, Δz_{Max}, and μ) on the JRC of 3D rock joint models, respectively. For this scenario, the length and width of the 3D rock joint models are equal to 100 mm. The modelling parameters related to the joint persistence are K_0 = 100%, P_{Drb} = 0, and P_{Grb} = 0. The remaining parameters are presented in Table 1. It can be seen here that six different sets of values are taken for each variable to investigate the effect on the JRC. Additionally, it should be noted that the JRC obtained from a single joint model is not representative due to the randomness of the joint surface morphology. The JRC presented in this section is the mean of the JRC obtained from the five joint models, based on the same modelling parameters.

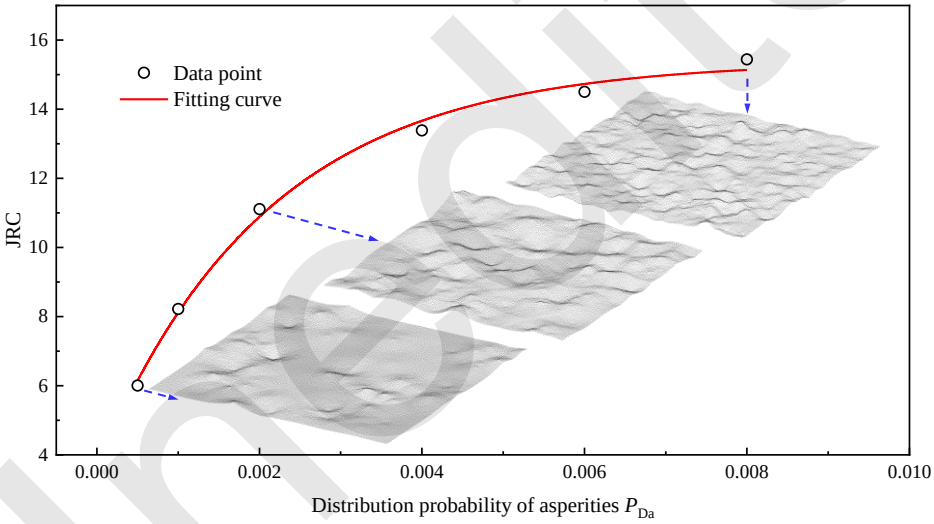

Fig. 5 The effects of the distribution probability of asperities (P_{Da}) on the JRC.

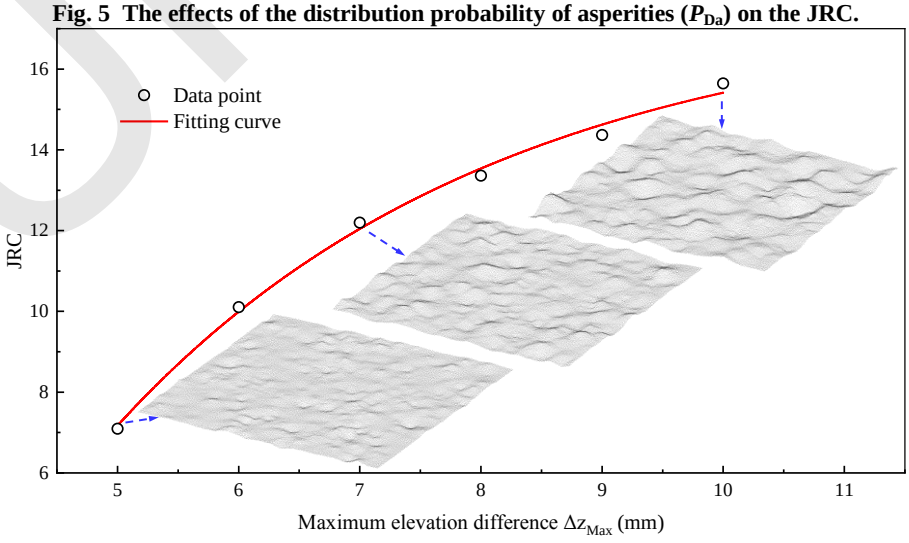

Fig. 6 The effects of the maximum elevation difference (Δz_{Max}) on the JRC.

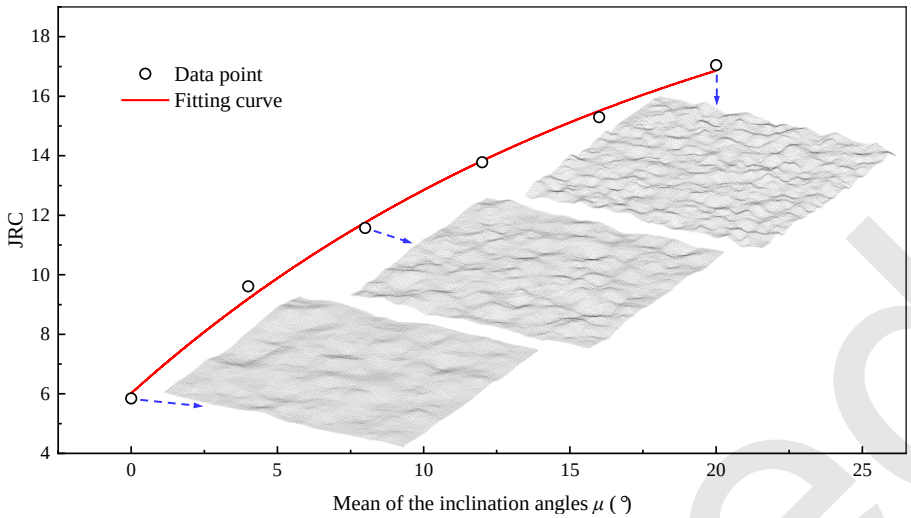

Fig. 7 The effects of the mean of the inclination angles (μ) on the JRC

Table 1 Parameters used in the models

Variable	No.	Δz_{Max} (mm)	Inclination angle		P_{Da}	P_{Ga}
			μ (°)	σ		
P_{Da}	P_{Da}-1	8	2	10	0.0005	0.8
	P_{Da}-2	8	2	10	0.001	0.8
	P_{Da}-3	8	2	10	0.002	0.8
	P_{Da}-4	8	2	10	0.004	0.8
	P_{Da}-5	8	2	10	0.006	0.8
	P_{Da}-6	8	2	10	0.008	0.8
Δz_{Max}	Δz_{Max}-1	5	2	10	0.004	0.8
	Δz_{Max}-2	6	2	10	0.004	0.8
	Δz_{Max}-3	7	2	10	0.004	0.8
	Δz_{Max}-4	8	2	10	0.004	0.8
	Δz_{Max}-5	9	2	10	0.004	0.8
	Δz_{Max}-6	10	2	10	0.004	0.8
μ	μ-1	6	0	5	0.004	0.8
	μ-2	6	4	5	0.004	0.8
	μ-3	6	8	5	0.004	0.8
	μ-4	6	12	5	0.004	0.8
	μ-5	6	16	5	0.004	0.8
	μ-6	6	20	5	0.004	0.8

Note: Δz_{Max} is the maximum elevation difference of a joint surface; the value of Δz_{Max} is equal to the difference between the maximum elevation of asperities and the minimum elevation of asperities; P_{Da} is the distribution probability of asperities; P_{Ga} is the growth probability of asperities.

Fig. 5 shows the effects of the distribution probability of asperities (P_{Da}) on the JRC of the 3D rock joint models. According to the six data points and the fitting curve, one can see that the JRC of the 3D rock joint models increases as the P_{Da} increases. Meanwhile, the rate of increase of the JRC decreases as the P_{Da} increases. The JRC of the 3D rock joint models increases faster when P_{Da} is less than 0.004 and slower when P_{Da} is greater than 0.004. Moreover, Fig. 5 also shows the 3D rock joint models with P_{Da} values of 0.0005, 0.002, and 0.008. As can be seen from the model diagrams, the number of asperities on the rock joint surfaces significantly varies. For the model with the P_{Da} of 0.0005, the number of asperities on the rock joint surface is the least among the three models. Many nearly-flat regions can also be

observed in this model. Compared with the other two models, the JRC of this model is the smallest. For the model with the P_{Da} of 0.008, the number of asperities on the rock joint surface is the largest, and the JRC of this model is the greatest among the three models. For the model with P_{Da} equal to 0.002, both the number of asperities and the JRC are the middle values among the three models. Fig. 5 shows that the method proposed in this paper can adjust the number of asperities by modifying the parameter P_{Da}, which effectively controls the JRC of the 3D rock joint models.

Fig. 6 shows the effects of the maximum elevation difference of the joint surface (Δz_{Max}) on the JRC of the 3D rock joint models. From the six data points and the fitting curve, it is clear that the JRC of the 3D rock joint models increases as Δz_{Max} increases. Meanwhile, the rate of increase of the JRC decreases slightly as Δz_{Max} increases. Furthermore, Fig. 6 shows the 3D rock joint models with Δz_{Max} values of 5 mm, 7 mm, and 10 mm. It can be seen that the height of the asperities on the rock joint surfaces differs significantly. For the model with a Δz_{Max} of 5 mm, the height of the asperities on the rock joint surface is the least among the three models. A simple visual evaluation indicates that this model has a lower roughness compared to the other two models. This quantitative comparison also indicates that the JRC of this model is the smallest among the three. For the model with a Δz_{Max} of 10 mm, the height of the asperities on the rock joint surface is the largest and the JRC of this model is the greatest. For the model with Δz_{Max} equal to 7 mm, both the height of the asperities and the JRC are the middle values among the three models. Fig. 6 shows that our proposed method can adjust the height of asperities by modifying the parameter of Δz_{Max}, which effectively controls the JRC of the 3D rock joint models.

Fig. 7 shows the effects of the mean of the asperity inclination angles (μ) on the JRC of the 3D rock joint models. By observing the six data points and the fitting curve, one can see that the JRC of the 3D rock joint models increases as μ increases. Meanwhile, the slope of the fitting curve decreases slightly as the μ increases. Fig. 7 also shows the 3D rock joint models with μ values of 0 °, 8 °, and 20 °. It can be seen that the slope of the asperities on the rock joint surfaces varies considerably. For the model with a μ value of 0 °, the slope of the asperities on the rock joint surface is the least among the three models. By visual observation and quantitative comparison, we can determine that the JRC of this model is the smallest among the three models. For the model with μ equal to 20 °, the slope of the asperities on the rock joint surface is the largest, and the JRC of this model is the largest among the three models. For the model with a μ value of 8 °, both the slope of asperities and the JRC are the middle values among the three models. Fig. 7 shows that the method proposed in this paper can adjust the slope of the asperity by modifying the parameter μ, which enables control of the JRC of the 3D rock joint models.

Fig. 8 shows the 3D non-persistent rock joint models with three different values of joint persistence (80%, 60%, and 40%) and the distribution probability of rock bridges (with P_{Drb} = 0.0002, 0.0005, and 0.001). In this scenario, the length and width of the 3D rock joint models both equal 100 mm. The modelling parameters related to the joint roughness are P_{Da} = 0.002, P_{Ga} = 0.8, Δz_{Max} = 8 mm, μ = 2 °, and σ = 10. The growth probability of the rock bridges is P_{Grb} = 0.03. It can be seen in Fig. 8 that the number and the area of rock bridges on the 3D non-persistent joint surfaces are different depending on the values of joint persistence and P_{Drb}. The white areas shown in the models represent the distribution areas of rock bridges. Figs. 8a-8c show 3D non-persistent rock joint models with joint persistences of 80%, 60%, and 40%, respectively. One can observe that the total area of the rock bridges increases as the joint persistence decreases. The total area of the rock bridges for the model shown in Fig. 8a is the smallest, while that of the model shown in Fig. 8c is the largest. For a certain degree of the joint persistence, the total area of rock bridges is nearly constant. The number of rock bridges increases and the area of the individual rock bridge decreases as P_{Drb} increases. For a certain degree of P_{Drb}, the number of rock bridges is nearly constant. Additionally, the joint persistence increases as the area of the individual rock bridge increases. Fig. 8 shows that the number of rock bridges on the joint surface can be controlled by adjusting the parameter P_{Drb}. The joint persistence can be tuned by adjusting the number and the area of rock bridges on the 3D non-persistent joint surface.

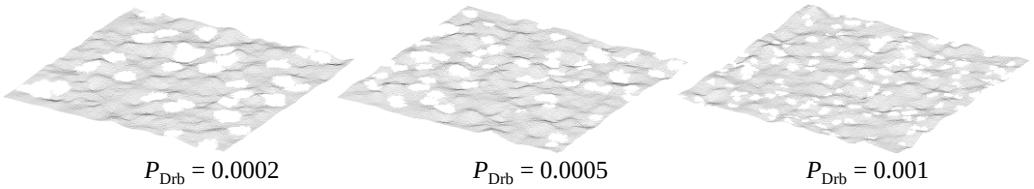

(a) Joint persistence = 80 %

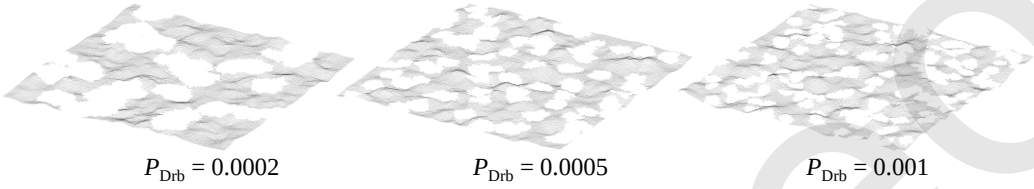

(b) Joint persistence = 60 %

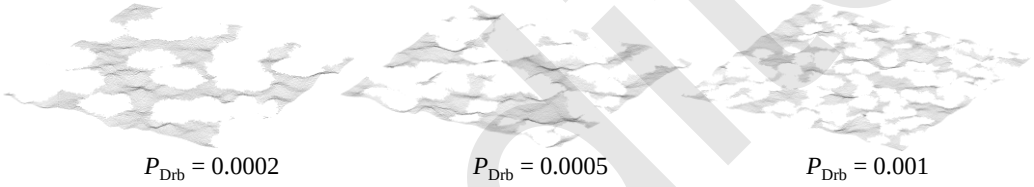

(c) Joint persistence = 40 %

Fig. 8 3D rock joint models with different joint persistence values and distribution probabilities of rock bridges (PDrb). (a) 3D rock joint models with joint persistence of 80%; (b) 3D rock joint models with joint persistence of 60%; (c) 3D rock joint models with joint persistence of 40%.

4 Validation

An artificially split joint was obtained by a splitting test and reconstructed with the proposed method to test the method's effectiveness. A cubic granite sample with a side length of 100 mm was selected for the test, as shown in Fig. 9a. The splitting test was carried out along the horizontal plane at the 50 mm height point of the rock sample. The length and width of the artificially split joint are both equal to 100 mm. Since the rocks on both sides of the artificially split joint surface are separated from each other, the joint persistence of the artificially split joint is equal to 100%. In order to obtain the morphological characteristics of this joint's surface, photographs were taken of the split rock sample from different viewpoints. The angles between adjacent viewpoints were less than 15°. The resolution of the camera is 1280 × 1024. Over 300 photographs were taken from different viewpoints to ensure that every detail of the split rock sample surface was captured. These photographs were imported into the software Reality Capture to generate a 3D digital model, as shown in Fig. 9b. Subsequently, the 3D coordinates for any position on the model surface were extracted based on computer-aided design (CAD) techniques. A total of 201 profiles were selected at 0.5 mm intervals on the joint surface, and 201 data points were selected at 0.5 mm intervals on each profile. The 3D coordinates of all data points were recorded. The elevation of the data point is defined as the relative elevation between the data point and the horizontal plane at the 50 mm height point of rock sample.

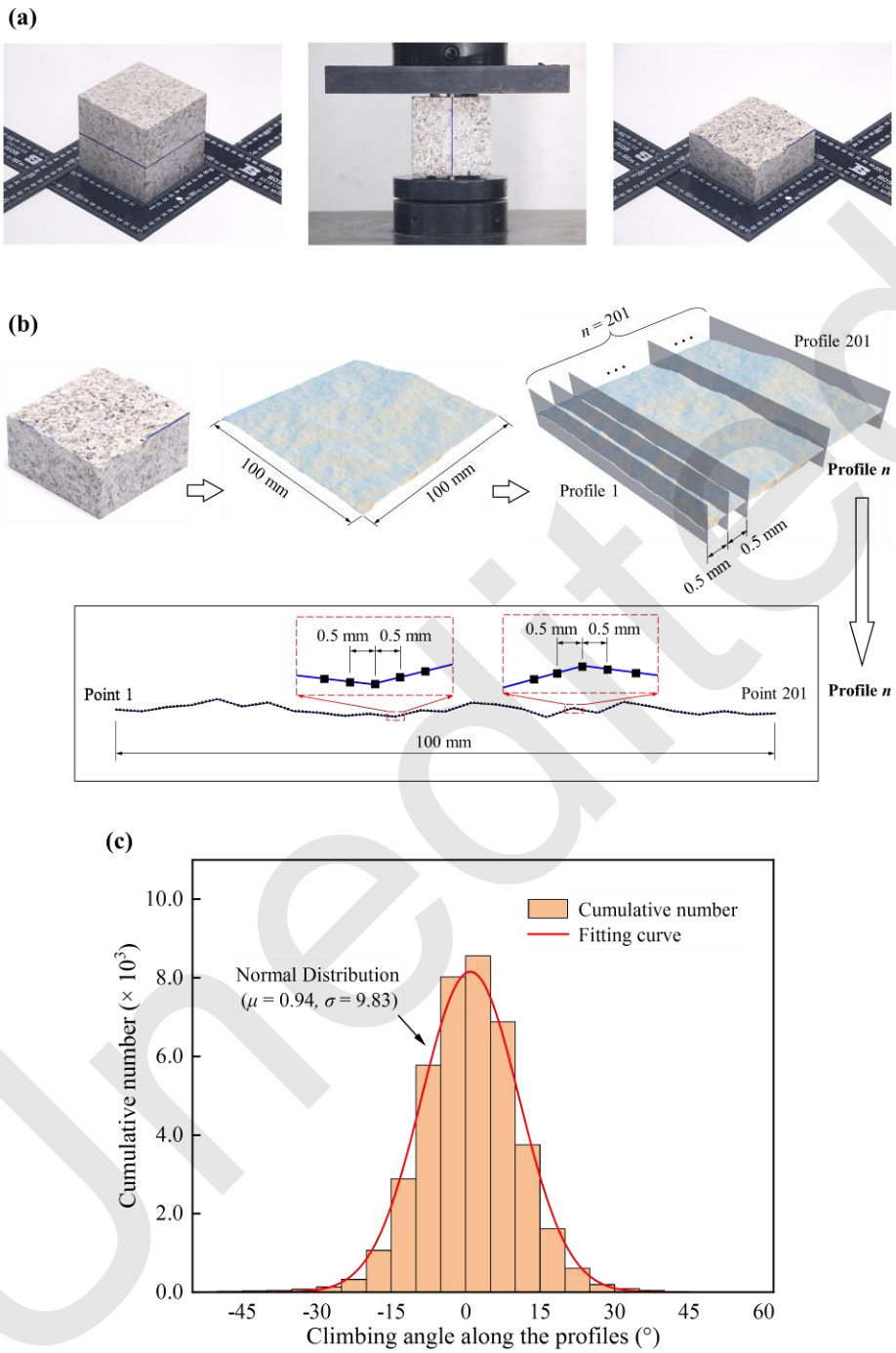

Fig. 9 Generation process and statistics of an artificially split joint. (a) The generation process of an artificially split joint by the splitting test; (b) Selection of profiles and data points; (c) The cumulative number of climbing angles from all profiles.

According to the 3D coordinates of the data points, the maximum elevation, minimum elevation, and the climbing angles along the profiles were counted. The maximum elevation of the joint surface is equal to 5.557 mm and the minimum elevation the joint surface is -3.075 mm. The maximum elevation difference of the joint surface is equal to 8.632 mm. The statistical results of the climbing angles along the profiles are presented in Fig. 9c. It can be seen that the climbing angles along the profiles approximately

follow a normal distribution. Based on the fitting curve, we estimate that the mean of the normal distribution is equal to 0.94, and the standard deviation is 9.83. Additionally, the JRC of the 3D joint surface is determined from the 201 profile lines. The quantification method of the JRC is the same as described in the previous section. The calculated JRC of the artificially split joint surface is equal to 8.13.

Based on the above statistical parameters, the artificially split joint is reconstructed using the proposed method. Fig. 10 shows the reconstructed models and the utilized modelling parameters. In addition to the statistical parameters mentioned above, the probability parameters for this reconstruction are P_{Da} = 0.002, P_{Ga} = 0.8, P_{Drb} = 0, and P_{Grb} = 0. Since a large number of random functions are used in the present method, a single reconstructed model is not representative of the whole. Thus, a series of 3D rock joint models are constructed based on the same modelling parameters. The accuracy of the method was evaluated by comparing the JRC of the reconstructed models with that of the artificially split joint. By a simple visual evaluation, we observe that three reconstructed models shown in Fig. 10 exhibit the similar joint roughness. Although the distribution of asperities is different for the reconstructed models, the number of the asperities, the slope of the asperities, and the maximum elevation difference of the reconstructed models are approximately the same. Meanwhile, the joint roughness of the reconstructed 3D rock joint models is similar to that of the artificially split joint.

No.	3D joint model	Parameters
Model Ⅰ		*Length* = 100 mm *Width* = 100 mm *Joint persistence* = 100 % *Maximum height of asperities* = 5.557 mm *Minimum height of asperities* = -3.075 mm *Inclination angle* $\mu = 0.94^{\circ}$, σ = 9.83 *Distribution probability* (*Rock bridge*) = 0 *Distribution probability* (*Asperities*) = 0.0012 *Growth probability* (*Rock bridge*) = 0 *Growth probability* (*Asperities*) = 0.8
Model Ⅱ		
Model Ⅲ		
…	…	

Fig. 10 3D rock joint models and the modelling parameters.

For a further quantitative comparison, the JRC of the reconstructed 3D rock joint models and that of the artificially split joint are calculated. Fig. 11 shows this comparison. It can be seen that the JRC of the reconstructed 3D rock joint models are similar to the JRC of the artificially split joint. The maximum value of JRC among the 10 data points shown in the figure is equal to 9.08, and the minimum value of JRC among the 10 data points is 7.52. The maximum difference between the JRC of the reconstructed models and the JRC of the artificially split joint is equal to 0.95. One can also observe that the majority of the data points fall within the error bands (±10%) of the JRC of the artificially split joint. This indicates that the JRC of the 3D rock joint models agrees with the JRC of the artificially split joint. Additionally, the JRCs of dif-

ferent reconstructed models generated using the same modelling parameters are approximately equal.

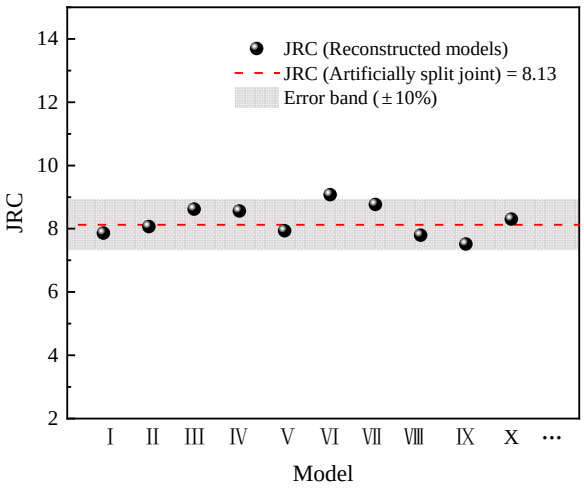

Fig. 11 The JRC of the reconstructed 3D rock joint models compared with the JRC of the artificially split joint.

5 Conclusions

A grid-growth method was proposed to reconstruct 3D rock joints with arbitrary joint roughness and persistence. The effects of the modelling parameters on the joint roughness coefficient and persistence were investigated, and the accuracy of the method was evaluated.

We showed that the proposed method can effectively control the JRC of joint models by adjusting the number, height, and slope of asperities. The parameters of P_{Da}, Δz_{Max}, and μ play a key role in this function. As the P_{Da} value increases, the number of asperities and the JRC of the joint models both increase. As Δz_{Max} increases, the height of asperities increases and the JRC of the joint models also increases. And as μ increases, both the slope of asperities and the JRC of the joint models increase.

The present method can effectively control the persistence of joint models by adjusting the number and area of rock bridges. As the total area of the rock bridges increases, the joint persistence of the models was found to decrease. Meanwhile, the total area of the rock bridges can be determined by the number of rock bridges and the area of each individual rock bridge.

Our novel method demonstrated high accuracy for 3D rock joint reconstruction. In a comparison, the JRC of the reconstructed models agreed with that of the artificially split surface. Additionally, the JRCs of different reconstructed models generated by the same modelling parameters were about equal.

This workflow was designed to construct 3D rock joint models with real morphologies. It provides accurate 3D rock joint models for numerical simulations, and is helpful in analyzing the effect of rock joint morphology on the mechanical properties of rock joint masses. However, this method is somewhat limited when it comes to complex cases, for instance where rock joints are offset from each other. Further investigations may be carried out to improve the method to account for such complexities.

Author contributions

Hanyu CHEN designed the research and wrote the original draft. Peng GUO helped to process the data and organize the manuscript. Guangyao LI helped with validation and investigation. Lifen FAN conceived the manuscript and provide the financial and resource support.

All authors have read and agreed to the published version of the manuscript.

Conflict of interest

The authors declare that they have no conflict of interest.

References

Askari M, Ahmadi M, 2007. Failure process after peak strength of artificial joints by fractal dimension. *Geotechnical and Geological Engineering*, 25(6):631-637. https://doi.org/10.1007/S10706-007-9135-6

Bae DS, Kim KS, Koh YK, et al., 2011. Characterization of joint roughness in granite by applying the scan circle technique to images from a borehole televiewer. *Rock Mechanics and Rock Engineering*, 44(4):497-504. https://doi.org/10.1007/s00603-011-0134-9

Bahaaddini M, Hagan P, Mitra R, et al., 2016. Numerical Study of the Mechanical Behavior of Nonpersistent Jointed Rock Masses. *International Journal of Geomechanics*, 16(1):04015035. https://doi.org/10.1061/(ASCE)GM.1943-5622.0000510

Barton N, Choubey V, 1977. The shear strength of rock joints in theory and practice. *Rock Mechanics and Rock Engineering*, 10(1-2):1-54. https://doi.org/10.1007/BF01261801

Cao RH, Yao RB, Lin H, et al., 2022. Shear behaviour of 3D nonpersistent jointed rock-like specimens: Experiment and numerical simulation. *Computers and Geotechnics*, 148:104858. https://doi.org/10.1016/j.compgeo.2022.104858

Cattania C, Segall P, 2020. Precursory Slow Slip and Foreshocks on Rough Faults. *Journal of Geophysical Research: Solid Earth*, 126(4):e2020JB020430.

https://doi.org/10.1029/2020JB020430

Einstein HH, Ventziano D, Beacher GB, et al., 1983. The effect of discontinuity persistence on rock slope stability. *International Journal of Rock Mechanics and Mining Sciences*, 20(5):227-236. https://doi.org/10.1016/0148-9062(83)90003-7

Gao Y, Wong LNY, 2015. A modified correlation between roughness parameter Z_2 and the JRC. *Rock Mechanics and Rock Engineering*, 48(1):387-396. https://doi.org/10.1007/s00603-013-0505-5

Gentier S, Riss J, Archambault G, et al., 2000. Influence of fracture geometry on shear behavior. *International Journal of Rock Mechanics and Mining Sciences*, 37(1-2):161-174. https://doi.org/10.1016/S1365-1609(99)00096-9

Ghazvinian A, Sarfarazi V, Schubert W, et al., 2012. A Study of the Failure Mechanism of Planar Non-Persistent Open Joints Using PFC2D. *Rock Mechanics and Rock Engineering*, 45(5):677-693. https://doi.org/10.1007/s00603-012-0233-2

Guan D, Wu JH, Jiang L, 2015. A statistical method for predicting sound absorbing property of porous metal materials by using quartet structure generation set. *Journal of Alloys and Compounds*, 626(25):29-34. https://doi.org/10.1016/j.jallcom.2014.11.159

Huang JY, Xu SL, Hu SS, 2014. Numerical Investigations of the Dynamic Shear Behavior of Rough Rock Joints. *Rock Mechanics and Rock Engineering*, 47(5):1727-1743. https://doi.org/10.1007/s00603-013-0502-8

Huang D, Tang W, Li XQ, 2023. Numerical modeling and damage evolution research on the effect of joint geometrical parameters in nonpersistent jointed rock masses. *Bulletin of Engineering Geology and the Environment*, 82(4):137. https://doi.org/10.1007/s10064-023-03143-1

Heike W, Simon L, Erik E, et al., 2008. Internal structure and deformation of an unstable crystalline rock mass above Randa (Switzerland): part I - internal structure from integrated geological and geophysical investigations. *Engineering Geology*, 101(1-2):1-14. https://doi.org/10.1016/j.enggeo.2008.01.016

Jiang Q, Feng XT, Gong YH, et al., 2016. Reverse modelling of natural rock joints using 3D scanning and 3D printing. *Computers and Geotechnics*, 73:210-220. https://doi.org/10.1016/j.compgeo.2015.11.020

Jimenez-Rodriguez R, Sitar N, 2006. Inference of discontinuity trace length distributions using statistical graphical models. *International Journal of Rock Mechanics and Mining Sciences*, 43(6):877-893. https://doi.org/10.1016/j.ijrmms.2005.12.008

Kim BH, Cai M, Kaiser PK, et al., 2007. Estimation of block sizes for rock masses with non-persistent joints. *Rock Mechanics and Rock Engineering*, 40(2):169-192. https://doi.org/10.1007/s00603-006-0093-8

Lang YX, Liang ZZ, Dong Z, 2024. Three-dimensional finite element simulation and reconstruction of jointed rock models using CT scanning and photogrammetry. *Journal of Rock Mechanics and Geotechnical Engineering*, 16(4)1348-1361. https://doi.org/10.1016/j.jrmge.2023.08.008

Le KH, Huang WC, Liao MC, et al., 2018. Spatial characteristics of rock joint profile roughness and mechanical behavior of a randomly generated rock joint. *Engineering Geology*, 245(1):97-105. https://doi.org/10.1016/j.enggeo.2018.06.017

Lei QH, Latham JP, Tsang CF, 2017. The use of discrete fracture networks for modelling coupled geomechanical and hydrological behaviour of fractured rocks. Computers and *Geotechnics*, 85:151-176. https://doi.org/10.1016/j.compgeo.2016.12.024

Liu QS, Tian YC, Liu DF, et al., 2017. Updates to JRC-JCS model for estimating the peak shear strength of rock joints based on quantified surface description. *Engineering Geology*, 228(13):282-300. https://doi.org/10.1016/j.enggeo.2017.08.020

Liu RC, Jiang YJ, Li B, et al., 2015. A fractal model for characterizing fluid flow in fractured rock masses based on randomly distributed rock fracture networks. *Computers and Geotechnics*, 65:45-55. https://doi.org/10.1016/j.compgeo.2014.11.004

Liu SL, Wang CS, Du SG, et al., 2022a. 3D morphology reconstruction of rock joints from 2D profile measurement by a profilograph. *Measurement* 203(5):112008. https://doi.org/10.1016/j.measurement.2022.112008

Liu XG, Zhu WC, Liu YX, et al., 2022b. Reconstruction of rough rock joints: 2D profiles and 3D surfaces. *International Journal of Rock Mechanics and Mining Sciences*, 156:105113. https://doi.org/10.1016/j.ijrmms.2022.105113

Liu ZQ, Zheng LL, Zuo YJ, et al., 2024. Investigation of three-dimensional model reconstruction and fractal characteristics of crack propagation in jointed sandstone. *Geomechanics and Geophysics for Geo-Energy and Geo-Resources*, 10(1):75. https://doi.org/10.1007/s40948-024-00797-3

Maerz NH, Franklin JA, Bennett CP, 1990. Joint roughness measurement using shadow profilometry. *International Journal of Rock Mechanics and Mining Sciences & Geomechanics Abstracts*, 27(5):329-343. https://doi.org/10.1016/0148-9062(90)92708-M

Marache A, Riss J, Gentier S, et al., 2002. Characterization and reconstruction of a rock fracture surface by geostatistics. *International Journal for Numerical and Analytical Methods in Geomechanics*, 26(9):873-896. https://doi.org/10.1002/nag.228

Nie ZH, Wang X, Huang DL, et al., 2019. Fourier-shape-based reconstruction of rock joint profile with realistic unevenness and waviness features. *Journal of Central South University*, 26(11):3103-3113. https://doi.org/10.1007/s11771-019-4239-8

Olsson O, Falk L, Forslund O, et al.,1992. Borehole radar applied to the characterization of hydraulically conductive fracture zones. *Geophysical Prospecting*, 40:109-142.

https://doi.org/10.1111/j.1365-2478.1992.tb00367.x

Prudencio M, Van Sint Jan M, 2007. Strength and failure modes of rock mass models with non-persistent joints. *International Journal of Rock Mechanics and Mining Sciences*, 44(6):890-902. https://doi.org/10.1016/j.ijrmms.2007.01.005

Shang J, West LJ, Hencher SR, et al., 2018. Geological discontinuity persistence: Implications and quantification. *Engineering Geology*, 241(26):41-54. https://doi.org/10.1016/j.enggeo.2018.05.010

Song JJ, 2006. Estimation of areal frequency and mean trace length of discontinuities observed in non-planar surfaces. *Rock Mechanics and Rock Engineering*, 39(2):131-146. https://doi.org/10.1007/s00603-005-0060-9

Song LB, Jiang Q, Zhong Z, et al., 2022. Technical path of model reconstruction and shear wear analysis for natural joint based on 3D scanning technology. *Measurement*, 188:110584. https://doi.org/10.1016/j.measurement.2021.110584

Sturzenegger M, Stead D, 2009. Quantifying discontinuity orientation and persistence on high mountain rock slopes and large landslides using terrestrial remote sensing techniques. *Natural Hazards and Earth System Sciences*, 9(2):267-287. https://doi.org/10.5194/nhess-9-267-2009

Tatone BSA, Grasselli G, 2010. A new 2D discontinuity roughness parameter and its correlation with JRC. *International Journal of Rock Mechanics and Mining Sciences*, 47(8):1391-400. https://doi.org/10.1016/j.ijrmms.2010.06.006

Thomas H, Frank S, Wohnlich S, 2021. FSAT - A fracture surface analysis toolbox in MATLAB to compare 2D and 3D surface measures. *Computers and Geotechnics*, 132:103997. https://doi.org/10.1016/j.compgeo.2020.103997

Tronicke J, Knoll MD, 2005. Vertical radar profiling: influence of survey geometry on first-arrival traveltimes and amplitudes. *Journal of Applied Geophysics*, 57(3):179-191. https://doi.org/10.1016/j.jappgeo.2004.11.001

Tse R, Cruden DM, 1979. Estimating joint roughness coefficients. *International Journal of Rock Mechanics and Mining Sciences & Geomechanics Abstracts*, 16(5):303-307. https://doi.org/10.1016/0148-9062(79)90241-9

Wang M, Wang J, Pan N, et al., 2007. Mesoscopic predictions of the effective thermal conductivity for microscale random porous media. *Physical Review E*, 75:036702. https://doi.org/10.1103/PhysRevE.75.036702

Wang QF, Li CW, Zhao YC, et al., 2019. Study of gas emission law at the heading face in a coal-mine tunnel based on the Lattice Boltzmann method. *Energy Science & Engineering*, 8:1705-1716. https://doi.org/10.1002/ese3.626

Wang XG, Jia ZX, Chen ZY, et al., 2016. Determination of discontinuity persistent ratio by Monte-Carlo simulation and dynamic programming. *Engineering Geology*, 203(25):83-98. https://doi.org/10.1016/j.enggeo.2015.12.001

Wasantha PLP, Ranjith PG, Xu T, et al., 2014. A new parameter to describe the persistency of non-persistent joints. *Engineering Geology*, 181(1):71-77. https://doi.org/10.1016/j.enggeo.2014.08.003

Wu Q, Kulatilake PHSW, et al., 2011. Comparison of rock discontinuity mean trace length and density estimation methods using discontinuity data from an outcrop in Wenchuan area, China. *Computers and Geotechnics*, 38(2):258-268. https://doi.org/10.1016/j.compgeo.2010.12.003

Xue DJ, Liu YT, Zhou HW, et al., 2020. Fractal Characterization on Anisotropy and Fractal Reconstruction of Rough Surface of Granite Under Orthogonal Shear. *Rock Mechanics and Rock Engineering*, 53(7):1225-1242. https://doi.org/10.1007/s00603-019-01974-7

Yong R, Ye J, Li B, et al., 2018. Determining the maximum sampling interval in rock joint roughness measurements using Fourier series. *International Journal of Rock Mechanics and Mining Sciences*, 101:78-88. https://doi.org/10.1016/j.ijrmms.2017.11.008

Zhang XB, Jiang QH, Chen N, et al., 2016. Laboratory investigation on shear behavior of rock joints and a new peak shear strength criterion. *Rock Mechanics and Rock Engineering*, 49(9):3495-3512. https://doi.org/10.1007/s00603-016-1012-2

Zhao LH, Huang DL, Chen JY, et al., 2020. A practical photogrammetric workflow in the field for the construction of a 3D rock joint surface database. *Engineering Geology*, 279(20):105878. https://doi.org/10.1016/j.enggeo.2020.105878

Zhou HW, Xie HP, 2003. Direct estimation of the fractal dimensions of a fracture surface of rock. *World Scientific Publishing Co Pte Ltd*, 10(5):751-762. https://doi.org/10.1142/S0218625X03005591

中文概要

题　目： 重构任意节理粗糙度和贯通度三维岩石节理的网格生长方法

作　者： 陈含宇，郭鹏，李光耀，范立峰

机　构： 北京工业大学，建筑与土木工程学院，中国北京，100124

目　的： 岩石节理面的形貌对节理岩体的力学特性具有重要的影响。本文旨在提出一种重构真实三维岩石节理形貌的方法，实现快速重构任意节理粗糙度和贯通度下的三维岩石节理，为节理岩体力学特性分析提供更为精确的模型。

创新点： 1. 提出了一种三维岩石节理重构的网格生长伐；

2. 同时考虑了三维岩石节理的节理粗糙度和贯通度；3. 基于该方法成功重构了人工劈裂节理。

方　法： 1. 将节理模型划分为均匀的网格，通过调整网格位置重构具有任意节理粗糙度和贯通度的岩石节理模型（图 1-3）；2. 建立不同节理粗糙度和贯通度的岩石节理模型，研究相关参数（如凸体的数量、高度和坡度，以及岩桥的数量和面积）对节理粗糙度系数（JRC）和贯通度的影响（图 4-8）；3. 重构人工劈裂节理，通过对比重构模型的 JRC 与人工劈裂节理的 JRC，验证了所提方法的可行性和有效性（图 9-11）。

结　论： 1. 本方法可以通过调节凸体的数量、高度和坡度来有效控制模型的节理粗糙度；2. 本方法可以通过调节岩桥的数量和面积来有效控制模型的节理贯通度；3. 基于本方法重构的节理模型与人工劈裂节理模型在节理粗糙度上吻合良好，本方法在三维岩石节理重构方面具有较高的准确性。

关键词： 三维岩石节理重构；节理粗糙度；节理贯通度；凸体；岩桥